Hindawi
International Journal of Antennas and Propagation
Volume 2020, Article ID 2719656, 9 pages
https://doi.org/10.1155/2020/2719656

Research Article

Application of Plasmonic Nanoantennas in Enhancing the Efficiency of Organic Solar Cells

Marcelino L. C. da Silva Jr., Victor Dmitriev, and Karlo Q. da Costa

Federal University of Para, Belem, PA, Brazil

Correspondence should be addressed to Marcelino L. C. da Silva Jr.; marcelinojr@ufpa.br

Received 27 July 2019; Revised 2 December 2019; Accepted 16 January 2020; Published 10 March 2020

Academic Editor: Mauro Parise

It is known that the periodic use of silver nanoantennas in organic solar cells increases the efficiency of light absorption. In this study, we performed a geometric parametric analysis of nanoantennas using the finite element method. Based on the study of the convex truncated cone nanoantenna, we have found that a nanoantenna arrangement formed by the convex truncated cone nanoantenna along with a pyramidal nanoantenna provides a better solution for different angles of light incidence compared to a single nanoantenna. We obtained a mean increase in the absorption efficiency of this organic solar cell, both for the TM and TE polarizations, compared to the use of the conventional nanoantenna in the wavelength range of 300–800 nm.

1. Introduction

Currently, organic photovoltaic systems perform at very different levels of development; such devices convert sunlight into electricity from organic semiconductors that constitute the active layer of these devices, which are generally composed of fullerene (C60) derivatives and conjugated polymers. Despite the mentioned advantages, organic solar cells (OSCs) do not have the efficiency to compete with silicon-based solar cells. Recently, a device that achieved efficiency of 17.3% in energy conversion [1] was presented, one of the largest ever achieved. In addition, for further developments in OSC-related research, there is a need for studies of the plasmonic effect with the insertion of metal nanostructures to improve the performance and stability of OSCs, as presented in [2], where it achieved the efficiency of 17.8% with the use of nanowires in the OSC.

The structural configurations of plasmonic nanostructures and device performance can be monitored from the photophysical properties of the system because the charge transfer dynamics and detailed plasmonic processes can be investigated. Thus, steady-state photophysics is a powerful tool for unraveling the plasmonic nature and revealing its plasmonic mechanisms [3–6]. The importance of this work is based on the fact that OSCs are receiving a lot of interest because of their potential with the use of metallic nanostructures deposited on them. Therefore, the present work aims to present and analyze a model of OSCs with influence of nanoantennas with good performance and to investigate improvements in these photovoltaic devices, having as challenge the development of a new solar cell that has greater efficiency in the region of the emitted light spectrum.

The structure of an OSC sensitized by a plasmonic nanoantenna, being excited by a variation of an external electric field, will be demonstrated to further analyze the photophysics and the efficiency of absorption in frequencies of the emitted spectrum. For this, some essential general aspects of the proposed plasmonic structure will be presented, and, later, the results obtained will be analyzed. First, we will apply the study in the OSC with the convex truncated cone nanoantenna (CNV) (Figure 1(a)), which was numerically simulated by means of the finite element method (FEM) through commercial software COMSOL Multiphysics [8]. Figure 1(b) shows the system is illuminated from the top with a linearly polarized plane wave with variation of the angle of incidence (θ) with respect to the z-axis. This wave has excitation at 800 nm away from the OSC. It is

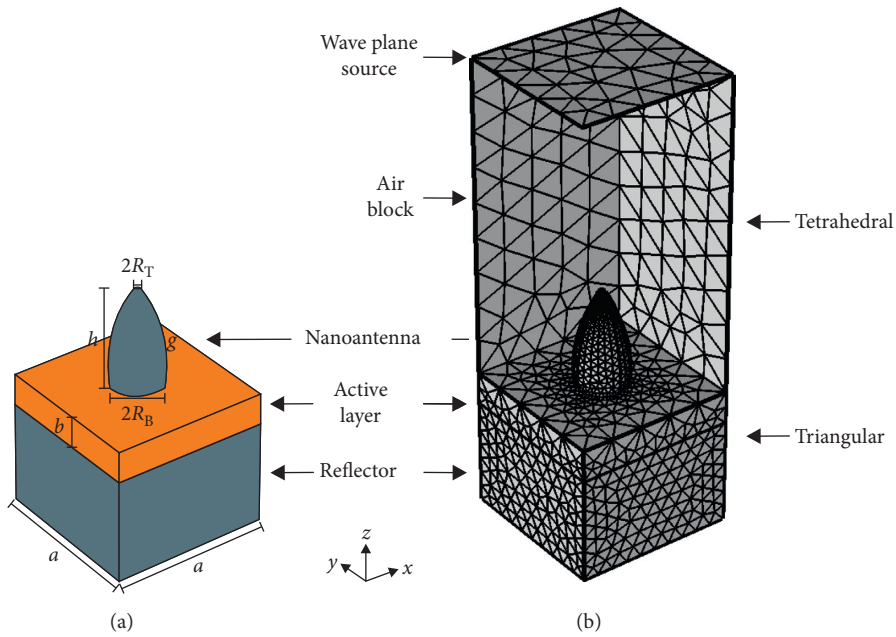

Figure 1: (a) Schematic diagram of the OSC with the CNV nanoantenna [7] and (b) OSC font and mesh definition.

configured using the interface *Electromagnetic Waves, Frequency Domain-emw*. The incident electric field is formed by expression $e^{(-i*k_x*x)} * e^{(-i*k_y*y)}$, at where $k_x = k_0 * \sin(\theta) * \cos(\phi)$ and $k_y = k_0 * \sin(\theta) * \sin(\phi)$ for electric field components E_0 that were entered in the *Electric mode field* in function *Port*, and the amplitude of the incident electric field is 1 V/m.

Also in Figure 1(b), the combination of tetrahedral and triangular meshes was used to take complete control over the characteristics of the defined device. The volume of geometries, including the nanoantenna, used the tetrahedral mesh, with a differentiation in the size of the mesh elements; in the air block, the maximum element size is 68.8 nm, and in the rest of the geometry, the maximum size is 30.1 nm. Then, a parametric analysis will be implemented for nanoantenna arrangement in the OSC set that will provide greater efficiency in the photovoltaic device.

2. Structure and Methods

The materials used in the OSC will be characterized by the electrical permissivity tensor (ε_r). The reflecting block and the nanoantenna are composed of silver, and they are characterized from the Drude model, with values for the variables according to [9].

$$\varepsilon_r(\omega) = 1 - \frac{\omega_p^2}{\omega(\omega - j\gamma)}, \quad (1)$$

where ω_p is the plasma bulk frequency e and γ is the electron shock ratio, i.e., losses in the metal. If we neglect the losses in the metal ($\gamma = 0$), we can see that $\omega > \omega_p$, and then the permissiveness is positive and light can propagate through the metal with a dispersion ratio given by

$$\omega^2 = \omega_p^2 - c^2 \cdot k^2, \quad (2)$$

where c is the velocity of light in the vacuum and k is the wave propagation constant.

For the active layer, the compound P3HT:PCBM is used, which possesses suitable morphology (formation structure) in the donor and acceptor regions. In addition, its distribution of phases occurs within the active layer. Due to the low diffusion length of the exon in organic materials, it is essential that adequate distribution be obtained for both phases, which leads to an increased interfacial area within the active layer mixture. Therefore, the material having relative permissiveness (ε_r) will be modeled according to experimental values, as shown in Figure 2 [10].

The parameters that describe the unit cell are the network constant (a), whose value is equal to 300 nm; the thickness of the reflecting layer, having a value equal to 200 nm; the thickness of the active layer (b), with a value of 60 nm; the height of the nanoantenna (h) is equal to 180 nm; the radius of the base (R_B) has a value of 44.7 nm; the top radius (R_T) has a value of 7, and the generatrix (g) has been defined as varying from 5 nm to 90 nm for both x and z coordinates of the control point $P1$ (x, z) of the Bézier curves [11], as shown in Figure 3.

In order to quantify the spectrum of the electromagnetic wave absorbed in the active layer of the OSC ($A(\lambda)$), i.e., the flux of electromagnetic energy transported through the polymer volume, we integrate the Poynting vector ($\vec{S}$) only in the region of the incident spectrum in the OSC.

The Poynting vector is defined as the cross product of real electromagnetic fields [12]:

$$\vec{S} = \vec{E}(\vec{r}, tt) \times \vec{H}(\vec{r}, t). \quad (3)$$

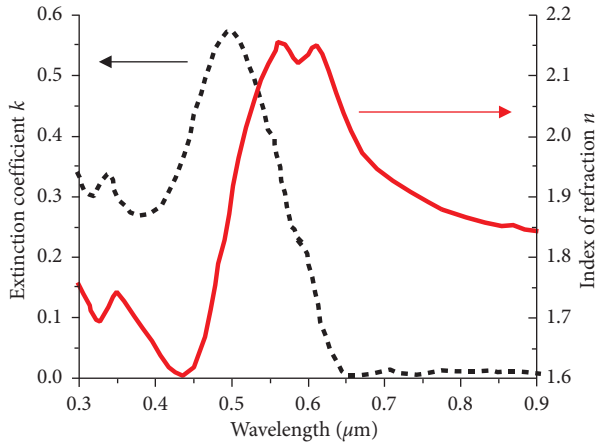

FIGURE 2: Optical constants of P3HT:PCBM with 1 : 1 weight ratio, and index of refraction n and extinction coefficient k are real [10].

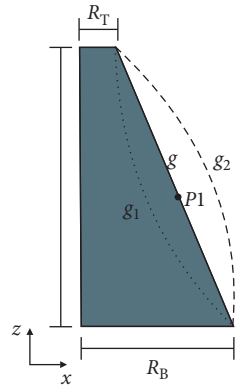

FIGURE 3: Side view geometries (only a half of the cross section is shown) and generatrices g, g_1, and g_2. For the convex truncated cone is g_2. The generatrices are defined by the Bézier curves with the quadratic order [11].

The direction ($\vec{S}$) is the propagation direction of the wave, in this case, a wave propagating in the positive direction along the z-axis. The complex electric field can be written as

$$\vec{E_c}(\vec{r},t) = \vec{E_0} e^{\frac{\pm\omega n_i z}{c}} e^{-l\omega\left(\frac{t\pm n_r z}{c}\right)}, \tag{4}$$

where the signal in the first exponential has to be negative to describe the decay of the wave amplitude due to the energy absorption by the medium. In addition, using the definitions to discuss electromagnetic fields in dispersive media, we focus on the monochromatic light with angular frequency (ω) and write the real electromagnetic fields, $\vec{E}$ and $\vec{H}$, as real parts of complex quantities.

$$\begin{aligned}\vec{S} = \frac{1}{4} e^{\frac{-2\omega n_i z}{c}} \Big[& \vec{E_0} \times \vec{H_0} e^{-2j\omega\frac{t\pm n_r z}{c}} + \vec{E_0^*} \times \vec{H_0} e^{0} \\ & + \vec{E_0^*} \times \vec{H_0^*} e^{2j\omega\frac{t\pm n_r z}{c}} + \vec{E_0} \times \vec{H_0^*} e^{0} \Big].\end{aligned} \tag{5}$$

When we measure this expression over time, the time-dependent terms tend to zero, and we obtain

$$S = \frac{1}{4} e^{(-2\omega n_i z)/c} \left[\vec{E_0} \times \vec{H_0^*} + \vec{E_0^*} \times \vec{H_0} \right] = \frac{1}{2} e^{(-2n_i z)/c} \mathrm{Re}\left[\vec{E_0} \times \vec{H_0^*} \right]. \tag{6}$$

Also, by using the time derivative in the Maxwell equation $\nabla \times \vec{E} = j\omega\mu\vec{H}$, we have

$$k \times \vec{E_c} = \omega\mu\vec{H_c}, \tag{7}$$

which together with equations $\begin{cases} \vec{E_c}(\vec{r},t) = \vec{E_0} e^{-j(\omega t \pm kr)} \\ \vec{H_c}(\vec{r},t) = \vec{H_0} e^{-j(\omega t \pm kr)} \end{cases}$ and the relations $\begin{cases} k \cdot \vec{E_c} = 0 \\ k \cdot \vec{H_c} = 0 \end{cases}$ produces amplitudes shown as follows:

$$\vec{H_0} = \left(\frac{k}{\mu\omega} \right) \vec{E_0}. \tag{8}$$

And for the cross product, $\vec{E_0} \times \vec{H_0^*} = (1/\mu\omega)|\vec{E_0}|^2 k^*$. By substituting in the equation of S, we find the magnitude of the Poynting vector with mean time:

$$S = \frac{1}{2\mu c} e^{(-2\omega n_i z)/c} n_r \left| \vec{E_0} \right|^2. \tag{9}$$

Lastly, $S(z) = (1/2) n_r |\vec{E_c}(z)|^2$.

Thus, the absorption of the electromagnetic wave in the active layer is calculated through the following equation:

$$A(\lambda) = \frac{\int_{300\mathrm{nm}}^{800\mathrm{nm}} \nabla \cdot S(z) \mathrm{d}V_{\mathrm{polymer}}}{P_{\mathrm{in}}}, \tag{10}$$

where P_{in} is the power incident at the OSC, which has the value expressed by the Poynting vector integral $S(z)$ about the source injection plan [13, 14].

$$P_{\mathrm{in}} = \frac{1}{2} \int \mathrm{Re} S(z) \cdot \mathrm{d}S. \tag{11}$$

The efficiency of this device via COMSOL Multiphysics [8], based on the equation, used the *Volume Integration* function in the *Derived Values* option in *Results*, where the polymer domain was selected and entered the function below in the field *Expression*:

$$\frac{d(\mathrm{real}(\mathrm{emw} \cdot \mathrm{Poavz}))}{P_{\mathrm{in}}}, \tag{12}$$

where Poav (*power flow, time average*), which is the energy flow with time average. The components x, y, and z of the Poynting vector are defined as *emw.Poavx*, *emw.Poavy*, and *emw.Poavz*, respectively. In order to quantify the absorptive capacity of the OSC structure in the region of the wavelength of interest, we defined an integrated absorption efficiency ($\mathrm{AE_{Int}}$) weighted and normalized with the input energy and the solar spectrum (air-mass 1.5G-AM1.5G) within the wavelength range of visible light (300–800 nm) [15, 16]. With the increase of activities for the development of SCs, the need to determine the spectral distribution of solar irradiation arose in order to characterize the OSCs and to compare the results in different parts of the world.

$$\mathrm{AE}_{\mathrm{Int}} = \frac{\int_{300\mathrm{nm}}^{800\mathrm{nm}} [P_{\mathrm{AM1.5G}}(\lambda) \times A(\lambda)]\,\mathrm{d}(\lambda)}{\int_{300\mathrm{nm}}^{800\mathrm{nm}} P_{\mathrm{AM1.5G}}(\lambda)\mathrm{d}(\lambda)}. \quad (13)$$

The choice of the wavelength region between 300 nm and 800 nm is relative to the absorbing properties of the active layer material.

Figure 4 shows the relation between the ultimate efficiency and the generatrix (g). In this investigation, the other parameters are taken as informed above. It should be noted that the absorption in OSC is dependent on the position of control point P1 (x, z). The study of the best position for P1 will accordingly broaden the bandwidth of the absorbed power and consequently the ultimate efficiency. It is thus found that the optimum efficiency of 82.5% is obtained, and then the value for these two points x e z in P1 (x, z) is equal to 72 nm.

Moreover, for the operation of OSCs under different irradiation conditions faced by stationary cells during the day, it is equally important to explore their performance under oblique incidence. In this regard, the development of a model for the operation of OSCs including the effect of angle of incidence is required. Therefore, Figure 5 shows $\mathrm{AE}_{\mathrm{Int}}$ (equation (13)) for various angles of incidence. It is worth noting that, for 45°, the efficiency of the nanoantenna was obtained with a low numerical value in relation to the other angles. Then, Figure 5 shows the values of $\mathrm{AE}_{\mathrm{Int}}$ for OSC with the CNV nanoantenna with the plane wave polarized in TM and TE.

It can be seen in Figure 5 that $\mathrm{AE}_{\mathrm{Int}}$ values are generally reduced to greater incidence angle (θ). There is a maximum absorption between the 10° and 15° angles of incidence for the TM and TE polarizations. This is because the surface area affected by the flat wave is larger in this range of angles, and the excitation conditions of the surface plasmon polariton waves are better.

Figure 6 shows the absorption versus wavelength map (λ) and incidence angle (θ), and it is noted that the analytical solution shown in Figure 5 correlates well since the position where the highest values of absorption were around the 15° angle. In addition, the absorption of the OSC with this nanoantenna acts significantly in the visible light range, operating in a wide range of wavelengths, which is highly desirable to improve the performance of the OSC.

Figure 7 shows the distribution of the electric field for the case CNV, where the color scale indicates the norm of the total electric field. We observed the highest concentration of the electric field at the base of the nanoantenna. This concentration is responsible for the increase of the electric field inside the active layer, which, consequently, increases the energy absorption by this active layer and, consequently, increases the efficiency of the OSC. A factor that justifies such field concentration is the curved shape of the nanoantenna that contributes to the formation of localized surface plasmon resonance (LSPR) [17].

The electric field strength variation at the interface between air and nanoantenna is shown in Figure 8. We observe that the electric field decays exponentially, that is, it is losing energy to the metal due to absorption. This behavior is a

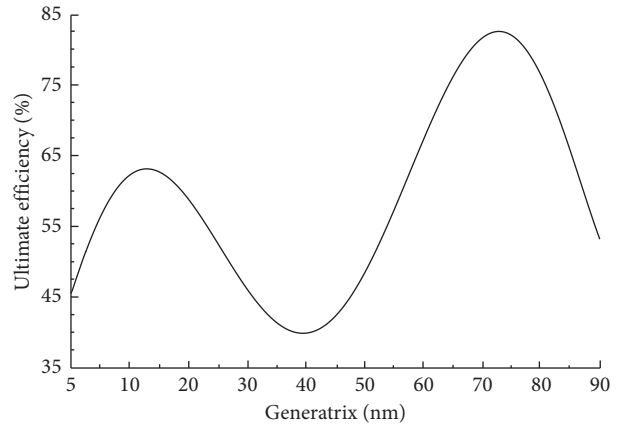

Figure 4: Absorption efficiencies of OSC as a function of generatrix.

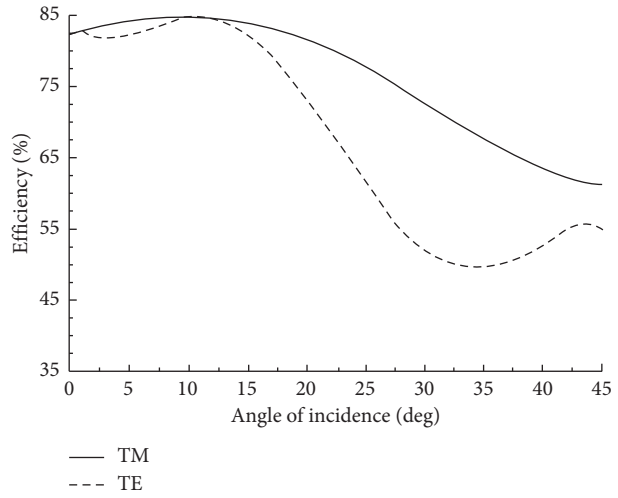

Figure 5: Integrated absorption efficiency ($\mathrm{AE}_{\mathrm{Int}}$) for OSC with the optimized CNV nanoantenna [7].

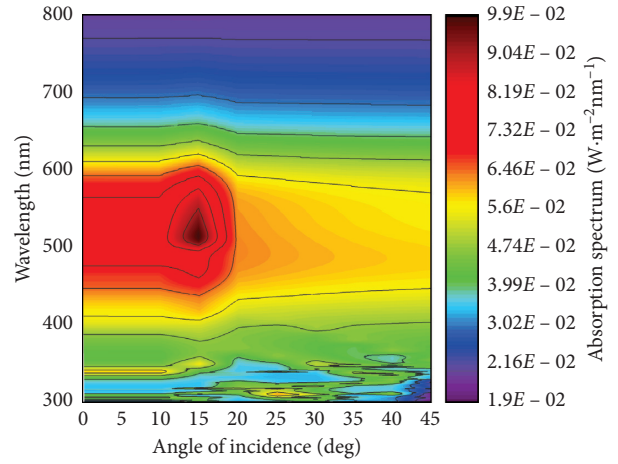

Figure 6: Map of the absorption in the OSC versus wavelength (λ) and incidence angles (θ).

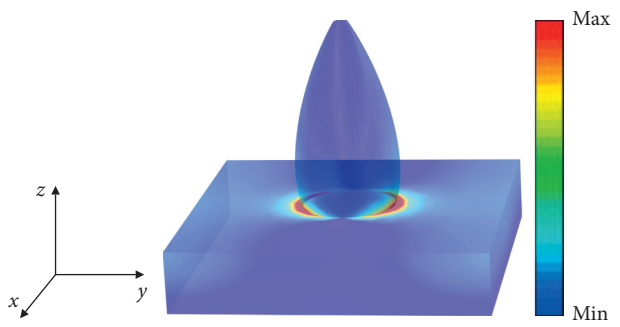

Figure 7: Field concentration in the CNV nanoantenna for normal incidence.

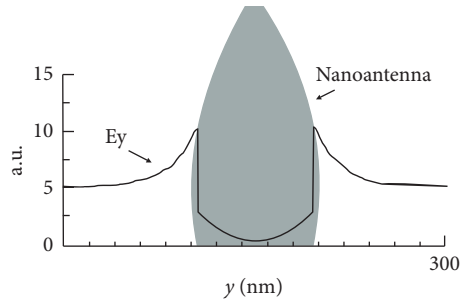

Figure 8: Electric field distribution near the nanoantenna for the CNV case and normal incidence.

characteristic of the symmetric pair coupled modes of surface plasmon polaritons (SPP) [18, 19].

In [20], the authors demonstrate the use of Ag nanoantenna cylindrical (Figure 9(a)) increased by up to 22% for both TM and TE polarizations. The modeling method was applied to the cylindrical nanoantenna, and the absorption result is shown in Figure 9(b).

We observe in Figure 9(b) showing normalized absorption that the maximum absorption is at $\lambda = 495$ nm, which corresponds to the resonance of the cylindrical nanoantenna related to its height (h) and radius (R) [20]. To verify this statement, we calculated the nanoantenna resonance by the developed method of moments (MoM) code of [21], where the nanoantenna is excited by plane wave in free space. The main absorption resonance obtained is at $\lambda = 497$ nm, which is in good agreement with the resonance of Figure 9(b). This shows that the main peak of absorption of Figure 9(b) is due to the resonance of the nanoantenna. Therefore, the method used in OSC with the CNV nanoantenna has been validated.

3. Results and Comments

Based on the above study, the formation of LSPR depends on the geometry of the nanostructure. Optical absorption reaches its maximum at the plasmonic resonance frequency. Figure 9 shows the extinction efficiency (i.e., cross-sectional to effective area ratio) of silver nanoparticles having different shapes. The peak position of the LSPR is very sensitive to the shape of the nanostructure.

Therefore, based on the analysis of Figure 10, to increase the operating wavelength range of the OSC with the CNV nanoantenna, a parametric analysis was implemented in the whole of the OSC with the inclusion of a nanoantenna in the form of a pyramid, which can provide a gain in the efficiency of the device. Thus, to meet the conditions of the parametric analysis, rigorous 3D simulations were done with the aim of maximizing the absorption efficiency. Figure 11 presents the parameters that will be optimized since both the shape and the dimensions of the metallic nanostructures are the main factors and determine the effectiveness of OSC. For the parameters of the pyramidal nanoantenna (PYR) are changed together in a given range of analysis.

The parametric analysis of the nanoantenna PYR was made from the parameter height (h) and edge of the base (R_B).

In addition, since the distance between the nanoantennas (d) is fundamental for the marriage of the resonance and thus to increase the absorption, the network constant (a) was optimized.

First, through the FEM, the analysis was performed between the ideal distance (d) between the nanoantennas, maintaining symmetry in the diagonal xy and the network constant (a) of the OSC, see Figure 12.

Thus, the following result (Figure 13) is obtained for the nanostructure. It is evident that the ideal values for the parameters d and a are, respectively, 148 nm and 340 nm.

Continuing the parametric analysis, several simulations were made in the OSC in order to find the ideal values for the set of parameters of the nanoantenna PYR, also with the normal incidence angle, that result in a higher value of AE_{Int}. The best results for AE_{Int} were with the parameters $h = 190$ nm and $R_B = 78.8$ nm. And in Figure 14, it shows that there is an increase in efficiency when pyramid top is 0.04, which is equal to 3.152 nm because it refers to the proportion of RB.

Figure 15 shows AE_{Int} (equation (13))for incident angles from 0° to 45° calculated in the OSC, with the system illuminated by a flat wave for both TM polarization and TE polarization.

This result shows that the use of the nanoantenna arrangement (CNV and PYR) in the OSC obtained better AE_{Int} values for angles greater than 25°. In a wide absorption bandwidth, corresponding to the solar spectrum with most of the solar energy, it indicates good performance in improving the absorption in photovoltaic devices.

Figure 16 shows the absorption versus wavelength map (λ) and incidence angle (θ), making evident the better performance of the OSC with the nanoantenna arrangement than with the use of the nanoantenna CNV. Absorption rates were better over the entire range of angle incident by the flat wave amplifying the absorption of the OSC in the visible light range, and with this nanostructure, the highest values of absorption are in the range of 12.5° to 32.5°.

As the arrangement of nanoantennas does not have radial symmetry, it was necessary to analyze by varying the Azimuth angle (φ) to understand the behavior of the nanostructure.

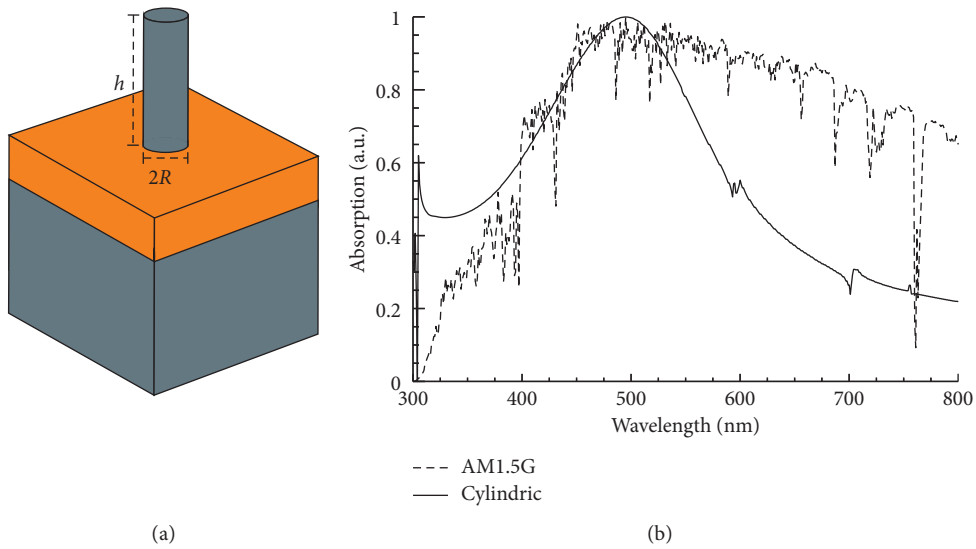

Figure 9: (a) Unit cell of the conventional OSC structure with the cylindrical nanoantenna. (b) Absorption $A(\lambda)$ for OSC with the optimized cylindrical nanoantenna related to absorption AM1.5G [20].

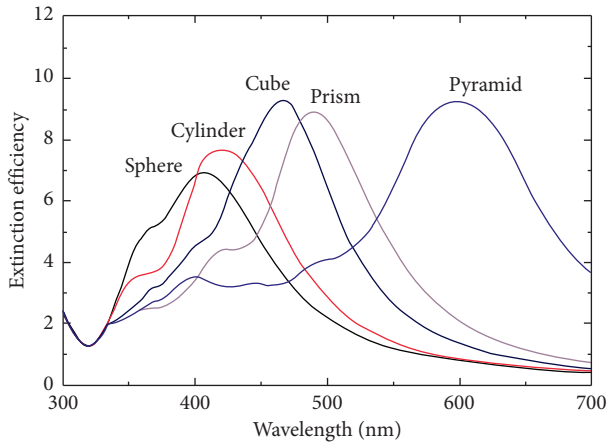

Figure 10: Efficiency of extinction of silver nanoparticles with different forms [15].

Figure 17 shows AE_{Int} for the same incidence range (0°–45°), with normal and polarized incidence in TM.

As can be seen in Figure 18, the greatest field concentration is present between the nanoantenna arrangement and the active layer, indicated with the red color according to the symmetry of the *xy* diagonal. Thus, the interaction with the electric field of the incident light is responsible for the appearance of the SPP resonance, making evident the formation of the oscillatory electric dipole in the CNV nanoantenna and the nanoantenna PYR according to the TM polarization of the incident plane wave.

The result obtained in the following (Figure 19) shows the evanescent decay of the electric field at the interface in the arrangement. This evanescent field correlates with the field concentration shown in Figure 18, justifying the field intensities concentrated at the base and top of the nanoantennas.

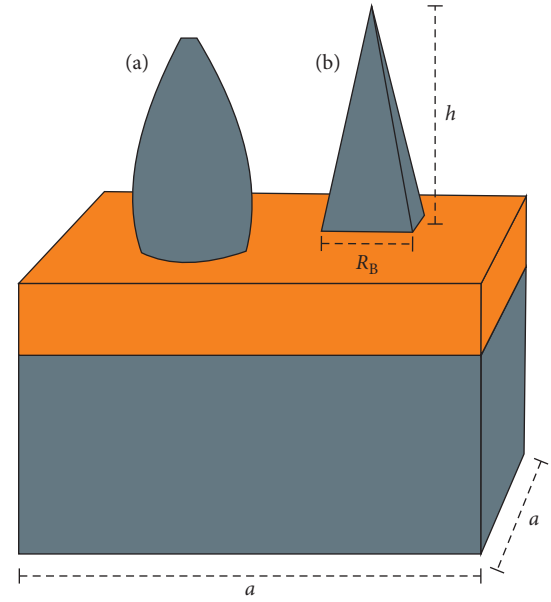

Figure 11: Arrangement of nanoantennas: (a) convex truncated cone (CNV) and (b) pyramidal (PYR).

The use of the nanoantenna arrangement maximized the concentration and scattering of incident light into the active layer at an angle different from the incident angle, increasing the wave propagation path (effective optical path) and light absorption.

Similar studies seeking improvements in OSCs from the dimensional characteristics of dielectric layer metal nanoantenna arrays [22–24] demonstrate experimental results proving increased efficiency. In these studies, the average behavior of devices in working region enhancement was discussed and is important for overall improvement. The discussion focuses on comparing the features of the nanoantenna arrangement over a thin dielectric film and air. By

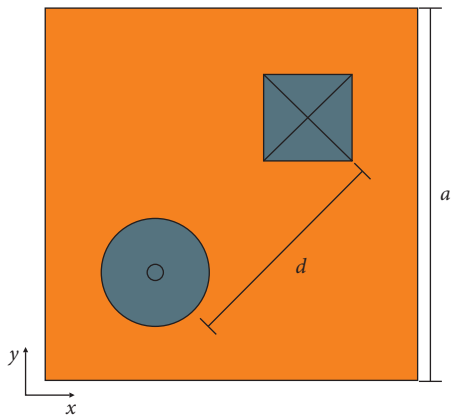

Figure 12: Positioning of the nanoantenna arrangement in the OSC (top view).

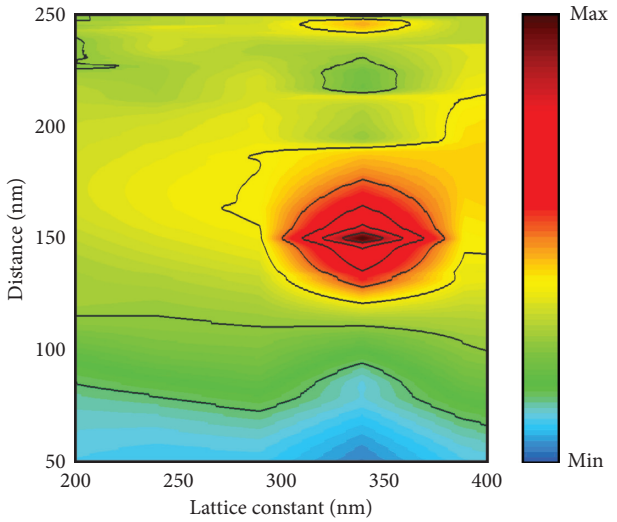

Figure 13: AE_{Int} in the active layer as function of (d, a).

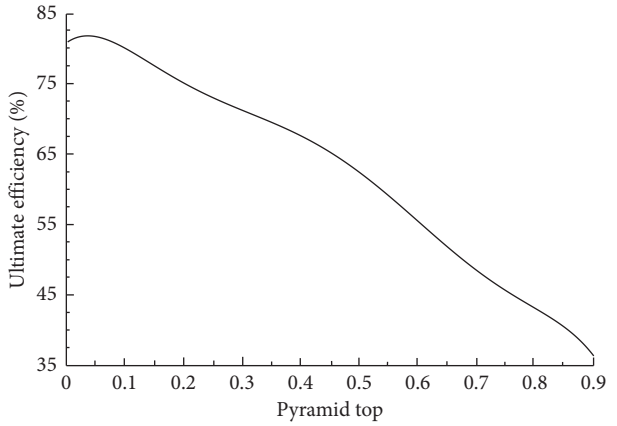

Figure 14: Absorption efficiencies of OSC as a function of pyramid top.

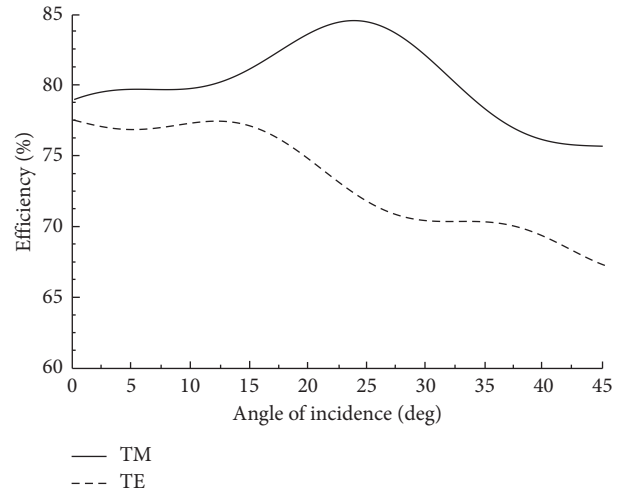

Figure 15: Integrated absorption efficiency (AE_{Int}) in relation to the angle of incidence (θ) for TM and TE biases.

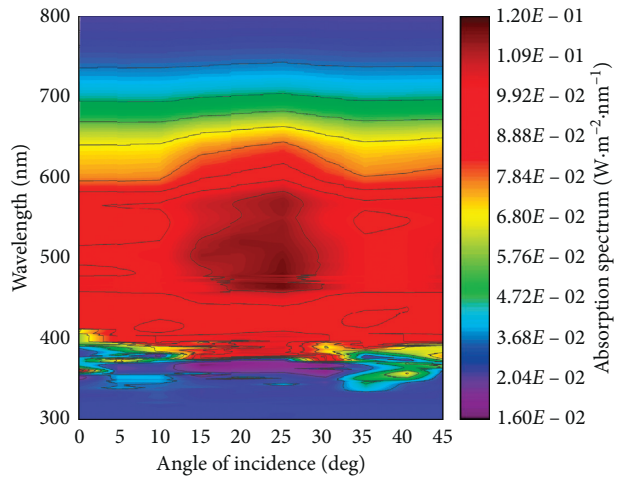

Figure 16: Map of the absorption in the OSC with arrangement of nanoantennas versus wavelength (λ) and incidence angles (θ).

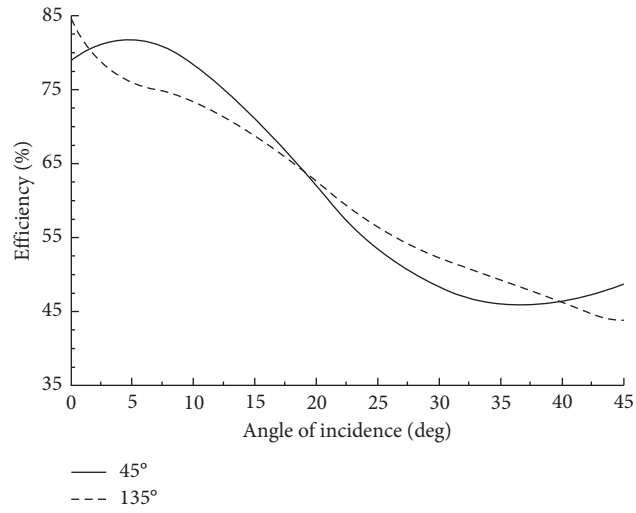

Figure 17: Integrated absorption efficiency (AE_{Int}) in relation to the angle of incidence (θ) for TM incidence and with equal Azimuth angles 45° and 135°.

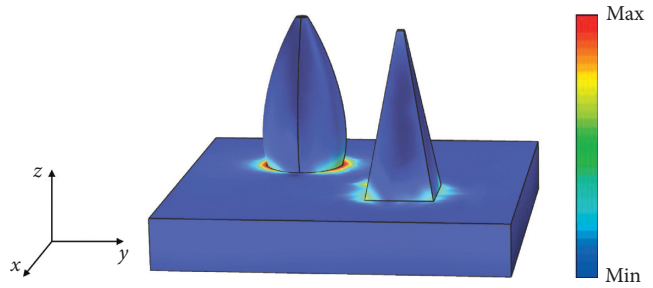

Figure 18: Field concentration in the arrangement of nanoantennas for normal incidence.

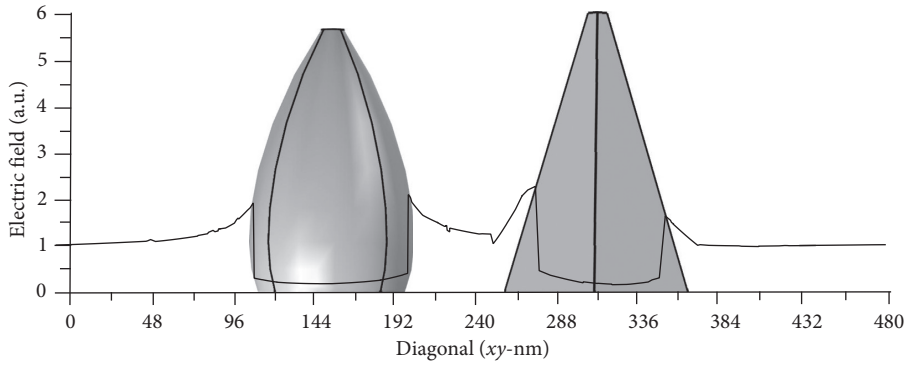

Figure 19: Plasmonic decay in the arrangement of nanoantennas for normal incidence.

the mean absorption of the 3D plots, in which the width, height, and space between the nanoantennas are controlled from the incident plane wave, the optimal size of paired strip nanoantennas can be realized.

4. Conclusions

In this work, we analyzed and enhanced periodic organic solar cells with the use of metallic nanoantennas to increase the absorption efficiency. The nanoantennas used are made of silver and placed above the active layer. Two different proposals were considered for the use of nanoantennas, the convex cone trunk and the convex cone trunk arrangement with pyramidal. Cells were illuminated by TM and TE with normal and oblique incidence. The finite element method was used for numerical simulations. The results show that the plasmonic solar cell with the use of the nanoantenna arrangement has a higher efficiency of absorption than the solar cell with the unitary nanoantenna. For example, we find an increase in the stability of the absorption efficiency of the nanoantenna arrangement than in the convex truncated cone nanoantenna for both TM and TE polarizations in the 300–800 nm wavelength range.

Data Availability

The data used to support the findings of this study are available from the corresponding author upon request.

Conflicts of Interest

The authors declare that they have no conflicts of interest.

Acknowledgments

This work was supported by Brazilian agencies CAPES and CNPq and PROPESP/UFPA.

References

[1] L. Meng, Y. Zhang, X. Wan et al., "Organic and solution-processed tandem solar cells with 17.3% efficiency," *Science*, vol. 361, pp. 1094–1098, 2018.

[2] J. E. M. Haverkort, E. C. Garnett, and E. P. A. M. Bakkers, "Fundamentals of the nanowire solar cell: optimization of the open circuit voltage," *Applied Physics Reviews*, vol. 5, pp. 031106-1–031106-22, 2018.

[3] L. Fenq, M. Niu, Z. Wen, and X. Hao, *Recent Advances of Plasmonic Organic Solar Cells: Photophysical Investigations*, MDPI, Basel, Switzerland, 2018.

[4] Z. Liang, J. Sun, Y. Jiang, J. Lin, and X. Chen, "Plasmonic enhanced optoelectronic devices," *Plasmonic*, vol. 9, no. 4, pp. 859–866, 2014.

[5] P. Shen, Y. Liu, Y. Long, L. Shen, and B. Kang, "High-performance polymer solar cells enabled by copper nanoparticles-induced plasmon resonance enhancement," *The Journal of Physical Chemistry C*, vol. 120, no. 16, pp. 8900–8906, 2016.

[6] L. Qiao, D. Wang, L. Zuo et al., "Localized surface plasmon resonance enhanced organic solar cell with gold nanospheres," *Applied Energy*, vol. 88, no. 3, pp. 848–852, 2011.

[7] M. L. C. Silva, V. Dmitriev, and K. Q. Costa, "Geometry optimization of plasmonic nanoantennas for organic solar cells," in *Proceedings of the International Microwave and Optoelectronics Conference*, Porto de Galinhas, Brazil, November 2015.

[8] COMSOL Multiphysics, The Platform for Physics-Based Modeling and Simulation, https://www.comsol.com/comsol-multiphysics.
[9] E. D. Palik, *Handbook of Optical Constants of Solids*, Academic Press, Cambridge, MA, USA, 1985.
[10] P. Muhlschlegel, H.-J. Eisler, O. J. F. Martin, B. Hecht, and D. W. Pohl, "Resonant optical antennas," *Science*, vol. 308, no. 5728, pp. 1607–1609, 2005.
[11] G. E. Farin, J. Hoschek, and M. Kim, *Handbook of Computer Aided Geometric Design*, vol. 4, pp. 75–109, Elsevier, Amsterdam, Netherlands, 2002.
[12] S. A. Maier, *Plasmonics: Fundamentals and Aplications*, Springer, New York, NY, USA, 2007.
[13] D. J. Griffiths, *Eletrodinâmica*, Pearson, London, UK, 3rd edition, 2011.
[14] M. N. O. Sadiku, *Elementos de Eletromagnetismo*, Bookman, Porto Alegre, Brazil, 3rd edition, 2004.
[15] C. Min, J. Li, G. Veronis, J.-Y. lee, S. Fan, and P. Peumans, "Enhancement of optical absorption in thin-film organic solar cells through the excitation of plasmonic modes in metallic gratings," *Applied Physics Letters*, vol. 96, no. 13, Article ID 133302, 2010.
[16] H. Shen and B. Maes, "Combined plasmonic gratings in organic solar cells," *Optics Express*, vol. 19, no. S6, p. A1202, 2011.
[17] B. Wu, N. Mathews, and T.-C. Sum, *Plasmonic Organic Solar Cells Charge Generation and Recombination*, Vol. 30, Springer, Berlin, Germany, 2017.
[18] X. H. Li, W. E. I. Sha, W. C. H. Choy, D. D. S. Fung, and F. X. Xie, "Efficient inverted polymer solar cells with directly patterned active layer and silver back grating," *The Journal of Physical Chemistry C*, vol. 116, no. 12, pp. 7200–7206, 2012.
[19] L. Zhou, X. Jiang, Y. Li et al., "Light extraction of trapped optical modes in polymer light-emitting diodes with nano-imprinted double-pattern gratings," *ACS Applied Materials & Interfaces*, vol. 6, no. 20, pp. 18139–18146, 2014.
[20] K. Q. Le, "Broadband light trapping in thin organic photovoltaic cells using plasmonic resonant antennas," *IEEE Journal of Photovoltaics*, vol. 6, pp. 1566–1569, 2013.
[21] K. Costa and V. Dmitriev, "Simple and efficient computational method to analyze cylindrical plasmonic nanoantennas," *International Journal of Antennas and Propagation*, vol. 2014, Article ID 675036, 8 pages, 2014.
[22] Z.-Y. Yang, C.-W. Su, and K.-P. Chen, "Optimization of effective absorption enhancement of paired-strips gold nanoantennas arrays in organic thin-films," *Applied Physics, A*, vol. 124, 2017.
[23] A. Mancini, V. Giliberti, A. Alabastri et al., "Thermoplasmonic effect of surface enhanced infrared absorption in vertical nanoantenna arrays," *Applied Physics, January*, vol. 122, no. 24, pp. 13072–13081, 2018.
[24] Y.-G. Bi, J. Feng, J.-H. Ji et al., "Nanostructures induced light harvesting enhancement in organic photovoltaics," *Nanophotonics*, vol. 7, no. 2, 2017.